

Flow and electrical anisotropy in the upper mantle: Finite-element models constraints on the effects of olivine crystal preferred orientation and microstructure

Alexander Gatzemeier, University of Göttingen, Institute of Geophysics, Göttingen, Germany
 Andréa Tommasi, Université Montpellier II, Laboratoire de Tectonophysique, Montpellier, France

SUMMARY

Long-period magnetotelluric (MT) data shows that electrical conductivity in the upper mantle is highly anisotropic. Agreement between high electrical conductivity directions and seismic anisotropy fast directions suggests that anisotropic diffusion of hydrogen along oriented olivine crystals controls the anisotropy of electrical conductivity in the upper mantle, since both seismic waves and hydrogen diffusion are faster along the [100] axis of olivine. Thus MT electrical anisotropy data, like seismic anisotropy, may be used to map flow patterns in the upper mantle. However, observed electrical anisotropies are significantly higher than seismic ones. To quantify the influence of strain-induced crystal preferred orientations of olivine on upper mantle bulk electrical conductivities, we calculate the macroscopic electrical conductivity anisotropy of a series of naturally and experimentally deformed peridotites using an anisotropic finite element model. These models, which fully take into account the microstructure: crystal and shape preferred orientations based on orientation maps obtained by indexation of electron back-scattered diffraction (EBSD) patterns, show macroscopic electrical anisotropy factors ranging from 3 to 16. The intensity of electrical anisotropy depends to first order on the intensity of the olivine crystal preferred orientations, but the relation saturates for strong crystal preferred orientations. In addition, the spatial distribution of the various crystal orientations may significantly enhance the anisotropy in strongly textured mantle rocks. The strongest anisotropy factors (>10) occur in mantle rocks in which deformation by dislocation creep has produced not only crystal but also strong shape preferred orientations, even if the latter is masked by recrystallization. Higher anisotropy factors (>100) observed in a few MT experiments imply however an additional, as yet unknown, mechanism controlling electrical conduction at asthenospheric depths in these regions.

Keywords: electrical conductivity, mantle anisotropy, hydrogen diffusivity, lattice-preferred orientation, finite-element modelling

INTRODUCTION

Long-period magnetotelluric (MT) data shows that electrical conductivity in the upper mantle, in particular in the asthenosphere, is highly anisotropic. Anisotropy factors (electrical anisotropy is defined as the ratio between highest and lowest electrical conductivity, $A = \sigma_{\max} / \sigma_{\min}$) obtained for sublithospheric depths (100-200 km) range, e.g., from >2 beneath central Australia (Simpson 2001) to >100 in Central Germany (Leibecker et al. 2002, Gatzemeier & Moorkamp 2005). Different processes may produce this anisotropy: (1) aligned melt lenses resulting from partial melting at the lithosphere-asthenosphere boundary, (2) aligned high-conducting films (e.g., graphite or sulphides) along grain boundaries, or (3) anisotropic diffusion of hydrogen (H+) along oriented olivine crystals.

Olivine is by far the most abundant (~50-70 vol.%) upper mantle mineral. As the principal interconnected phase, its conductivity is assumed to dominate the bulk conductivity of the upper mantle down to the transition zone at 410 km depth (e.g., Xu et al. 2000a). Moreover, agreement between electrical and seismic anisotropy fast directions (e.g., Ji et al. 1996, Eaton et al., 2004) suggests that seismic and electrical anisotropies have a common cause. Seismic anisotropy in the upper mantle is linked to coherent orientation of olivine crystals over length scales of tens to hundreds of kilometers in the upper mantle (e.g., Mainprice et al. 2000). Like the propagation of seismic waves (or polarization for shear waves), H+ diffusion is faster along the [100] axis of the olivine crystal (Mackwell and Kohlstedt 1998). Thus preferred orientation of olivine [100] axis may produce electrical anisotropy in the asthenosphere. Experiments at high temperature and moderate pressure, as well as extensive data on naturally

deformed mantle rocks show that olivine at upper mantle conditions deforms essentially by dislocation creep with dominant slip on the [100](010) system, developing strong crystal preferred orientations (CPO) characterized by alignment of the [100] axis with the flow direction and of the [010] axis normal to the flow plane (see review in Tommasi et al. 2000). Thus if H⁺ diffusion in olivine is the dominant electrical conductivity mechanism, fast electrical conductivity directions map flow directions in the asthenospheric mantle, similarly to fast shear wave polarizations or fast P- or Rayleigh waves propagation directions. The high electrical conductivities inferred at asthenospheric depths (≥ 0.1 S/m) (e.g., Lizarralde et al. 1995, Simpson 2001, Gatzemeier and Moorkamp 2005), which cannot be explained based on the electrical conductivity of dry olivine, provide evidence for a dominant role of H⁺ diffusion in olivine in the electrical conduction at these depths (Hirth et al. 2000). However, in contrast to observations on seismic, observed bulk electrical anisotropies (Simpson 2003, Gatzemeier and Moorkamp 2005) are significantly higher than expected from intrinsic crystal anisotropies. To verify if a given deformation may produce high enough electrical anisotropies, we study the electrical conductivity anisotropy at the sample scale. Indeed, a fundamental parameter to this question is how the electrical anisotropy produced by anisotropic H⁺ diffusion rates in individual olivine crystals is transferred to the polycrystal (rock) scale.

MODELLING ELECTRICAL PROPERTIES OF POLYCRYSTALLINE AGGREGATES

A large number of approaches may be used to predict effective electrical properties of composite media from the properties and distribution of its components, e.g., effective medium, percolation theory, random resistor networks. All these methods however do not take into account the microstructure of the samples. Here we calculate bulk electrical properties using finite element modeling.

In a 3D finite element model (FEM), the effective electrical conductivity tensor of a polycrystalline

Table 1 Crystal preferred orientations intensities (*J* factor), Voigt-Reuss-Hill (VRH, $A = \sigma_{max}/\sigma_{min}$), and finite element (FE) electrical anisotropies of the studied samples. For the FEM, we show the electric currents j_x, j_y, j_z and anisotropies $A = j_x/j_y$ that result from an applied electric field $E=(1, 1, 1)$.

Samples	J-index	Electrical anisotropies	
		VRH	FEM ($j_x/j_y/j_z/A$)
900A87-2	5.62	4.4	0.50/0.08/0.17/6.0
FRB1359	4.75	3.4	0.34/0.06/0.09/5.6
EPTA3	10.98	5.5	0.36/0.05/0.11/6.9
PO342	13.03	5.4	0.49/0.03/0.11/14.3

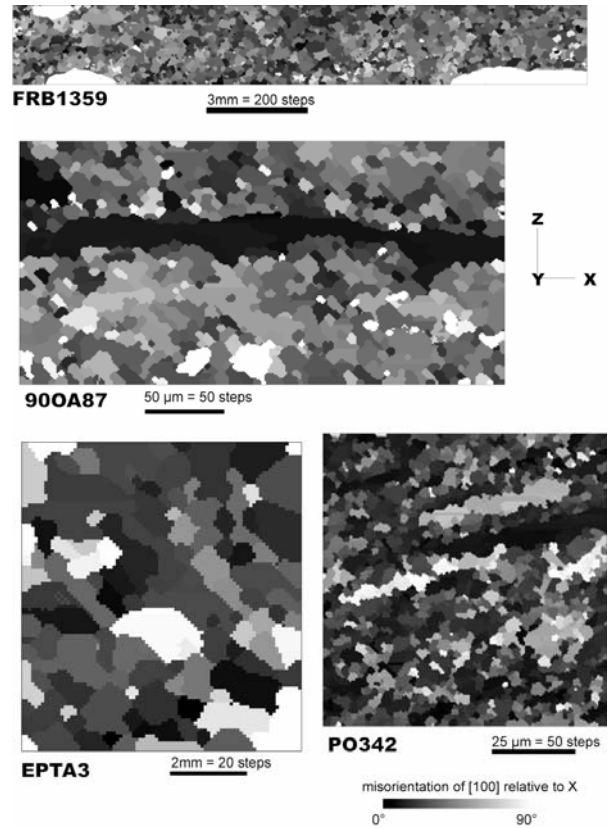


Figure 1 Crystallographic orientation maps obtained by indexation of electron backscattered diffraction (EBSD). Each step corresponds to an orientation measurement. Gray scale indicates the angular misorientation of the olivine [100] axis relative to the macroscopic X direction, which corresponds to the lineation (maximum grain elongation) in the naturally deformed peridotites FRB1359 and EPTA3, to the extension direction in harzburgite 900A87, and to the shear direction in dunite PO342. All maps were performed in the XZ structural plane, i.e., parallel to the flow direction and normal to the flow plane.

aggregate depends on the full microstructure, i.e., on the orientation and shape of the crystals that compose the aggregate, on their spatial distribution, and on their electrical conductivity tensors. The microstructural information for the aggregate is presented as a 2-D or 3-D digital image composed of square or cubic pixels, respectively (Fig. 1). To each pixel is associated data defining the mineral phase and the orientation of the crystallographic lattice relative to a macroscopic reference frame. Each grain is described by a set of neighbouring pixels with similar composition and orientation; a grain may be defined by up to several hundred pixels, depending on the resolution of the image. The crystal orientation data is used to orient the conductivity tensor of each pixel. Bulk electrical properties of the aggregate are then obtained using an

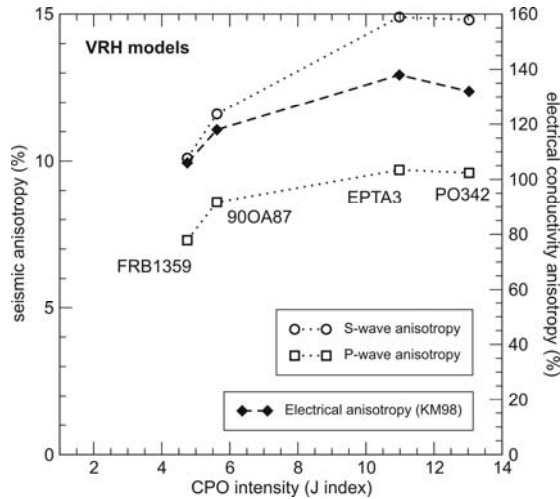


Figure 3 Seismic ($A_{max}\%=(V_{max}-V_{min})*100/V_{mean}$) and VRH electrical ($A_{max}\%=(\sigma_{max}-\sigma_{min})*100/\sigma_{mean}$) anisotropies as a function of the CPO intensity.

anisotropic finite-element modelling (FEM) by calculating the current densities that are produced by a constant electric field (Garboczi 1998). Since a detailed description of the microstructure is only available for the XZ plane (2D, Fig. 1) and the extension of the model in the third dimension is ensured essentially by the periodic boundary conditions, we only consider the current densities j_x and j_y in the sample plane. For the samples given Tab. 1 j_x and j_y are parallel to sample coordinates X and Z.

ELECTRICAL ANISOTROPY OF UPPER MANTLE ROCKS

Among all conduction mechanisms active in mantle rocks, we consider here only conduction due to hydrogen diffusion which, in the presence of water, is assumed to dominate mantle conductivity (e.g., Karato 1990). For olivine we use hydrogen diffusivities along the main crystallographic axes based on results of Kohlstedt & Mackwell (1998)

$$D_{[100]}^{ol} \approx 20 \times D_{[010]}^{ol} \approx 40 \times D_{[001]}^{ol} \quad (KM98)$$

and Nernst-Einstein equation (Karato 1990) to obtain the 3D electrical conductivity tensor.

Sample description

The studied peridotites display a wide range of microstructures (variations in grain size and shape, Fig. 1) that allows testing the effect of the microstructure on the electrical conductivity.

All samples show olivine crystal preferred orientations (CPO, Fig.2) characterized by a strong concentration of [100] parallel to the flow direction (inferred parallel to the lamination in the EPTA3 and FRB1359, observed extension or simple shear direction in 90OA87 and PO342, respectively). The [010] direction is aligned normal to the flow plane, with some dispersion in a plane normal to the flow direction in all samples except

from EPTA3. Olivine CPO intensities vary from sample to sample with FRB1359 displaying the weakest orientation and PO342 the strongest. The intensity of a CPO may be characterized by the integral of the orientation distribution function, the J factor, which varies from 1 for an isotropic aggregate to infinity for a single crystal (Bunge 1982). J factors in the studied peridotites range from 4.75 for FRB1359 and 13 for PO342 (Tab. 1). The peridotites selected for this study sample the entire range of CPO intensities usually observed in upper mantle rocks.

A first hint on the intrinsic anisotropy of a mantle peridotite may be obtained by the analysis of the bulk seismic properties and electrical conductivity tensors predicted by simple volumetric averaging methods, like the Voigt-Reuss-Hill (VRH) average (Hill 1952). The Voigt-Reuss-Hill (VRH) averaging provides a first approximation to the CPO-induced electrical anisotropy, which does not consider the effect of the microstructure. Discrepancy between VRH average and FEM anisotropy indicates therefore the influence of the microstructure, in this case connectivity of the high-conductivity phase (well-oriented grains) on bulk electrical properties. P-wave velocity, S-wave polarization anisotropy and electrical conductivity calculated using a VRH averaging based on the mineral composition and on the CPO of the studied peridotites are shown in Fig. 2.

Seismic anisotropy for both P- and S-waves does not display a linear dependence on CPO intensity, but a fast increase of anisotropy at low J factors and stabilization at J factors higher than 8 (Tommasi 1998). Electrical anisotropies obtained from VRH averages reveal a similar dependence (Fig. 3).

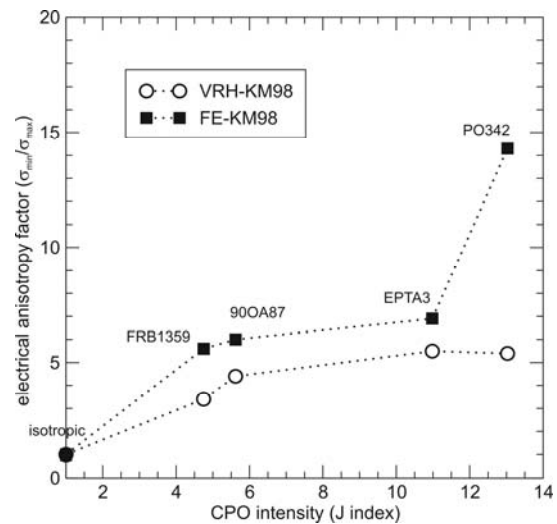


Figure 4. Electrical anisotropy factors calculated by VRH averaging (empty symbols) and by finite element modelling (full symbols) using KM98 for the different samples as a function of the olivine CPO intensity (J index).

FEM Results

A comparison of VRH and FEM results show that FE electrical anisotropy factors systematically exceed the VRH ones (Fig. 4). In general the FEM results confirm the tendency observed for the VRH averages of increasing electrical anisotropy with increasing CPO intensity. However the FEM results show that the spatial distribution and, hence, the interconnectivity of the various CPO components can significantly enhance the electrical anisotropy. A closer analysis of the FEM results for samples PO342 highlights the effect of these two parameters on the electrical anisotropy:

FEM anisotropies calculated for sample PO342 are ~3-fold those predicted by the VRH model. Indeed, EPTA3 and PO342 show a weak variation in J-factor that lead to similar values for P-, S-wave, and VRH electrical anisotropies (Fig.2), but differ significantly in their FE electrical anisotropies (Fig. 4). High (j_x) and low (j_y) current densities for PO342 in comparison with EPTA3 (Tab. 1) indicate significantly enhanced electrical conductivity along X and concurrent diminished conductivities along Y. This higher anisotropy may be explained by the microstructure of PO342 (Fig. 1), which is characterized by lenses of similar CPO very elongated parallel to the flow direction X (porphyroclasts or recrystallized domains that had originated from a single elongated porphyroclast). These highly elongated porphyroclasts correspond to grains in easy glide orientations, characterized by [100] semi-parallel to the shear direction (X). These lenses form thus a connected high-conductivity pathway along X and a low-conductivity pathway along Y, resulting in a much higher electrical anisotropy than the one that would be produced by a similar CPO with a random distribution of the various CPO components.

CONCLUSIONS

- Intensity of electrical anisotropy depends on a first order on intensity of olivine CPO.
- Comparing FEM with VRH averages shows that spatial distribution and especially interconnectivity of the various CPO components in mantle samples significantly enhances their electrical anisotropy.
- Strongest anisotropy factors (>10) should occur in mantle rocks in which deformation by dislocation creep has produced not only crystal but also strong shape preferred orientations, even if the latter is marked by recrystallization.

Significantly higher anisotropies observed in regions like central Germany (Gatzemeier & Moorkamp 2005) imply that H⁺ is not the dominating conduction mechanism. This suggests the existence of other, still unaccounted for, conduction mechanisms.

Because laboratory measurements have shown that magnesium diffusion along grain boundaries is more rapid than within olivine crystals (Farver et al., 1994), grain boundary diffusion of hydrogen might be a

mechanism as important as intracrystalline H⁺ diffusion. Further numerical simulations including grain boundary diffusion are currently under way.

ACKNOWLEDGEMENTS

We thank Misha Bystricky, Walid Ben Ismail, and Emmanuela Pera for providing the EBSD maps and David Mainprice for stimulating discussions and help with various coding problems. A.G was funded by a post-doctoral scholarship from the Deutsche Forschungsgemeinschaft.

REFERENCES

- Bunge, H.-J., 1982. *Texture Analysis in Materials Science*. Butterworth, London.
- Kohlstedt, D.L., Mackwell, S.J., 1998. Diffusion of hydrogen and intrinsic point defects in olivine. *Z. Phys. Chem.* 207, 147–162.
- Leibcker, J., Gatzemeier, A., Höning, M., Kurat, O., Soyer, W., 2002. Evidences of electrical anisotropic structures in the lower crust and the upper mantle beneath Rhenish Shield. *Earth Planet. Sci. Lett.* 202, 289–302.
- Lizarralde, D., Chave, A., Hirth, G., Schultz, A., 1995. Northeastern Pacific mantle conductivity profile from long-period magnetotellurics sounding using Hawaii-to-California submarine cable data. *J. Geophys. Res.* 100, 17837-17854.
- Mainprice, D., Barruol, G., Ben Ismail, W., 2000. The seismic anisotropy of the Earth's mantle: from single crystal to polycrystal, in *Earth's Deep Interior: Mineral Physics and Tomography from the Atomic to the Global Scale*, pp. 237-264, ed. Karato, S.I., AGU, Washington, DC.
- Eaton, D. W., Jones, A. G., Ferguson, I. J., 2004. Lithospheric anisotropy structure inferred from collocated teleseismic and magnetotelluric observations: Great Slave Lake shear zone, northern Canada. *Geophys. Res. Lett.* 31, L19614.
- Farver, J. R., Yund, R. A., Rubie, D. C., 1994. Magnesium grain boundary diffusion in forsterite aggregates at 1000°C-1300°C and 0.1 MPa to 10 GPa. *J. Geophys. Res.* 99, 19809-19819.
- Garboczi, E. J., 1998. *Finite Element and Finite Difference Programs for Computing the Linear Electric and Elastic Properties of Digital Images of Random Materials*. NIST, Internal Report 6269.
- Gatzemeier, A., Moorkamp, M., 2005. 3D modelling of electrical anisotropy from electromagnetic array data: hypothesis testing for different upper mantle conduction mechanisms. *Physics. Earth Planet. Int.* 149, 225-242.

Hill, R., 1952. The elastic behaviour of a crystalline aggregate. Proc. Phys. Soc. London A 65, 349-354.

Karato, S., 1990. The role of hydrogen in the electrical conductivity of the upper mantle. Nature 347, 272-273.

Hirth, G., Evans, R., Chave, A., 2000. Comparison of continental and oceanic mantle electrical conductivity: Is the Archean lithosphere dry?. Geochem. Geophys. Geosyst., 1:paper number 2000GC000048.

Tommasi, A., Mainprice, D., Canova, G., Chastel, Y., 2000. Viscoplastic self-consistent and equilibrium-

based modelling of olivine lattice preferred orientations. Implications for upper mantle seismic anisotropy. J. Geophys. Res. 105, 7893-7908.

Tommasi, A., 1998. Forward modeling of the development of seismic anisotropy in the upper mantle. Earth Planet. Sci. Lett. 160, 1-13.

Xu Y., Shankland, T. J., Duba, A. G., 2000a. Pressure effect on electrical conductivity in the Earth's mantle. Phys. Earth Planet. Int. 118, 149-161.

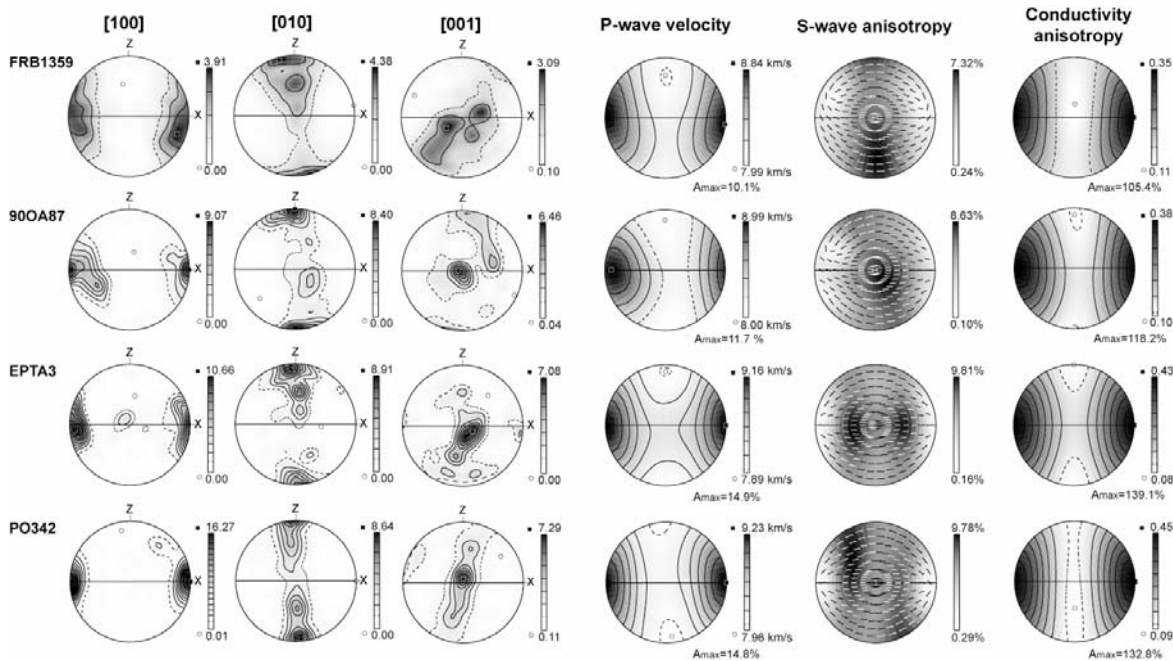


Figure 2. Olivine crystal preferred orientations and three dimensional distributions of P-wave velocity, S-wave polarization anisotropy, and electrical conductivity calculated by Voigt-Reuss-Hill averaging for the four studied peridotites. Electrical conductivity is calculated using the olivine H⁺ diffusion data of Kohlstedt and Mackwell (1998). Equal area projections, lower hemisphere. X marks the flow direction and Z the normal to the flow plane (also marked by the horizontal solid line). For seismic waves, $A_{max}\% = (V_{max} - V_{min}) * 100 / V_{mean}$. VRH electrical anisotropy is defined as $A_{max}\% = (\sigma_{max} - \sigma_{min}) * 100 / \sigma_{mean}$. Olivine CPO are contoured at 1 multiple of an uniform distribution intervals, P-wave velocities at 0.2 km/s intervals, S-wave anisotropy at 1% intervals. A_{max} is defined in the text. Electrical conductivity data is normalized relative to the conductivity in the olivine crystal along the [100] direction.

MAGNETOTELLURIC CATECHISM

Berdichevsky (1) and Dmitriev (2)
Moscow State University

1. Presently one cannot entrust the computer (even the supercomputer) with complete self-dependent automatic press-button inversion. Inversion should be conducted in the interactive mode realizing the contact between the geophysicist (a leader) and the computer (a performer). Leader suggests to performer an inversion strategy that can define the interpretation success. The inversion strategy can include the hypotheses testing.
2. The statement of the inverse problem calls for a normal background, which can be given as a mathematical abstraction consistent with magnetotelluric response functions obtained at the boundary of the observation area and with a priori information.
3. The inverse problem is unstable. Its solution is meaningful provided it is sought within a restricted set of plausible solutions forming the interpretation model. The choice of the interpretation model should be confidently controlled by a priori information and qualitative indications derived from the field observations.
4. The magnetotelluric field is of diffusive nature. Generally it can offer only a smoothed image of the geoelectric medium. Existing in the Earth buried sharp conductivity contrasts are introduced into the interpretation model using a priori information or hypothetically. The most complete interpretation can be performed by a compromise between smoothing (Occam) and contrasting (blocky) inversions.
5. In solving an unstable inverse problem, we come up against the paradox of instability. The more restricted the interpretation model, the more stable the inverse problem and the poorer the detailedness of its solution. On the other hand, the more stable the inverse problem, the higher its resolution. The resolution of the inverse problem and the detailedness of its solution are antagonistic. The inverse problem should be solved with optimum relation between stability, resolution and detailedness. An interpretation model with a small number of layers and structures is preferable. The additional layers and structures can be introduced providing the magnetotelluric and magnetovariational indications demand their presence. Taking advantage of blocky partition, a number of parameters defining the interpretation model should be reduced to a minimum conditioning a stable solution.
6. The magnetotelluric inverse problem is multicriterion. We can use tippers, magnetic tensors, impedance tensors, phase tensors. These response functions have different sensitivity to different parameters of the interpretation model and different immunity to near-surface distortions. The best approach to the solution of a multicriterion inverse problem is a succession of partial inversions focused upon different elements of the interpretation model. Partial inversions trade their information: the result of a previous inversion is transferred to a next inversion as a starting model. When studying media with sharp horizontal contrasts and strong geoelectric noise, it is profitable to begin with tippers which are free from static distortions and nicely resolve the geoelectric medium not only in the horizontal directions but in the vertical direction as well (!!!). It is just tipper that under complicated conditions can give a sound reliable basis for further estimates performed by phases and apparent resistivities.
7. The magnetotelluric effects are of integral nature and therefore the large compact bodies can manifest themselves as mosaic alternation of cells of higher and lower conductivity. Such a solution should be considered as one of the equivalent solutions. In agreement with geological expediency, it can be smoothed under condition that the misfits of the response functions do not increase.
8. The inversion adequacy should be estimated by comparing the modeled and measured local response functions. The model elements whose elimination does not increase the misfits of the response functions are considered as unnecessary insignificant artifacts and removed.
9. Magnetotelluric large-scale regional studies of sediments and deep studies of the Earth's crust and upper mantle are usually carried out on the long single profiles which dooms geophysicists to the quasi-one-dimensional or two-dimensional interpretation of the observation data. Admissibility of such simplifications should be verified by a priori and a posteriori analysis of lateral effects. An important part of this analysis is an appraisal and correction of interpretation errors arising due to finite strike of elongated structures considered as two-dimensional ones.

10. The main puzzle of magnetotellurics is a violation of the dispersion relations between apparent resistivities and impedance phases. We know from experience that this phenomenon occasionally happens and we have several mathematical models that expose this phenomenon. But we badly understand its physical mechanisms and we cannot tell with distinctness what properties of the geoelectric medium are responsible for it. The study in this field is a challenge for all of us.